Journal of Heat and Mass Transfer Research

Journal homepage: http://jhmtr.semnan.ac.ir

Semnan University

Experimental Investigation of Condensation Heat Transfer on Vertical Hydrophilic-Hydrophobic Aluminium Surfaces

Pouyan Mohseni Behbahani [*,a], Ghanbar Ali Sheikhzadeh [a,b]

[a]*Department of Thermofluids, Faculty of Mechanical Engineering, University of Kashan, Kashan 8731753153, Iran.*

[b]*Energy Research Institute, University of Kashan, Kashan 8731753153, Iran.*

PAPER INFO

Paper history:
Received: 2021-12-25
Revised: 2022-06-08
Accepted: 2022-06-12

Keywords:
Dropwise condensation;
Filmwise condensation;
Heat flux;
Heat transfer coefficient;
Hybrid hydrophobic-hydrophilic.

ABSTRACT

Condensation is an important heat transfer regime, with vast applications in industries such as power generation and cooling systems. In the present study, the changes in the coating thickness and geometry of hydrophobic areas were investigated on hydrophobic-hydrophilic plates and totally hydrophobic ones, and a no-coating plate was also studied experimentally for the condensation phenomenon. Considering the use of aluminium as the base material, tests such as lithography with positive photoresist was conducted to study the photoresist adhesion to the aluminium surface and its impact on heat transfer, as well as testing the lift-off process to remove the remaining photoresist at the final stage of producing the plates, to improve their surfaces and optimize the major parameters in the production stage. For this study, one type of totally hydrophobic surface and two types of hybrid hydrophobic-hydrophilic surfaces with different widths of hydrophobic and hydrophilic areas were produced, each type in three thicknesses of 200, 450 and 900 nm. Considering the different values of coating thicknesses, the width of the hydrophobic and hydrophilic areas, the heat transfer coefficient and heat flux were calculated for each plate, and the optimal conditions for each plate were determined. Compared to the uncoated plates, the heat transfer coefficient and heat flux for each plate with hybrid hydrophobic-hydrophilic surfaces (width of 860 μm for hydrophilic area and 970 μm for the hydrophobic, and thickness of 450 nm) registered increase by 1.44-2.01 and 1.43-1.81 times, respectively, which were the highest among the plates in the present study.

DOI: 10.22075/jhmtr.2022.25698.1369

1. Introduction

Condensation is an important heat transfer regime, which has vast applications in industries [1-4]. One of the most important issues in condensing and boiling regimes is the study of increasing heat transfer coefficient and heat flux [5-8]. The process of condensation on a surface can be categorized into filmwise and dropwise condensation. The type of condensation depends on wettability of the surface, and thus the energy and surface tension between the surface and condensed substance. In the filmwise condensation, the condensed liquid appears as a contiguous layer on the surface, while the dropwise condensation produces separate drops of the liquid with different dimensions on the surface. The filmwise condensation occurs for liquids with high adhesion to the surface, and the dropwise when condensed liquid is less inclined to such adhesion.

Schmidt et al. [9], for instance, observed a high heat transfer coefficient (HTC) for dropwise condensation (DWC), compared to filmwise condensation, leading many researchers to focus on DWC, such as Citakoglu and Rose [10], Izumi et al. [11], and Koch et al. [12], who reported increased water vapor condensation at a definite condensation degree on vertical beds.

[*]*Corresponding Author: Pouyan Mohseni Behbahani*
Email: pouyan_mohseni@yahoo.com

For instance, Majumdar and Mezic [13] conducted an experimental study on the performance of compressed steam condensers, and showed that the condenser performance to be improved when using certain chemicals a few millimeters wide as the hydrophobizing coating of the flow passage. Furthermore, Vemuri and Kim [14] performed an experimental condensation test using low-energy-level materials on various coating surfaces, and observed HTC enhancement and long-term DWC stability. For that purpose, a copper surface was coated with one-layer, N-octadecyl mercaptan, and stearic acid coatings, and HTC was reported higher by three times compared to the non-modified plain copper surface. In another experimental study by Tianqing et al. [15], it was shown that on-surface condensation did not initiate as dropwise and filmwise, and that the theory of nucleation sites served as the basis for the formation mechanism of DWC initial droplets. The majority of the recent analytical models assumed droplet formation at nucleation sites, the process of condensation on the free surface of droplets, small heat transfer between the droplets, and the heat transfer toward the solid surface through droplets towards as latent. For instance, Ma et al. [16] experimentally investigated DWC on a vertical plate in an environment of non-condensable gases, with values for saturation pressures, concentrations, and surface temperatures being different. For that purpose, a fluorocarbon coating was employed on the vertical plate, resulting in higher DWC. The dimensions of droplets about to fall were also suggested as a determining parameter to affect any rise in condensation HTC of steam. Boreyko and Chen [17], for example, identified DWC to be capable of continuous induction on a surface with no external forces. Therefore, droplets sweeping from the surface could be attributed to the released energy from the droplets combining with one another, whose released energy detached them from the surface at increased speed to 1m/s.

Taleshbahrami et al. [18] experimentally studied dropwise condensation on hydrophobic surfaces produced through a one-step electrodeposition process. The results showed that during the electrodeposition process, micro-nanostructures of copper were formed on the surface, and that controlling time and current positively affected the heat transfer in the dropwise condensation, in a manner that plates produced at low electrodeposition times (15 and 45 seconds) had lower dropwise condensation heat transfer than filmwise, while for higher times (135 seconds), the electrodeposition of dropwise condensation heat transfer at temperature differences below 10 K was 2-4 times higher than the filmwise condensation. Different methods have been proposed in books and studies for producing hydrophobic and super-hydrophobic surfaces, and recent laboratory research have inclined toward two-stage methods, such as generating surface roughness at micro- and nano-scales, and then reducing the surface energy to instigate hydrophobicity.

Many researchers, however, have recently been enticed in the coincidence of super-hydrophobic and super-hydrophilic characteristics on surfaces, such as Ghosh et al. [19], who investigated different hydrophilic−superhydrophilic patterns, and observed them to combine and sustain FWC and DWC on the substrate, respectively, thus reaching at a unique pattern for hydrophilic-superhydrophilic surface known as “bio-inspired interdigitated pattern”, which displayed a more favorable performance over straight hydrophilic-superhydrophilic design in conditions with higher humidity, and with non-condensable gases present. In another experimental work, Peng et al. [20] studied the increase in steam condensation heat transfer over hybrid hydrophobic-hydrophilic vertical plates, and observed that better condensation heat transfer performance at first on the hybrid surfaces due to increased width of the hydrophobic area up to a certain extent, yet being decreased afterwards, and settling at an optimum width of the hydrophilic areas. Furthermore, they depicted easier and more effective progress of steam condensation heat transfer through suitably-designed hybrid hydrophilic-hydrophobic surfaces. It was also reported by Peng et al. [21] that the hybrid dropwise and filmwise surface could successfully promote condensation heat transfer of steam, especially for condensing surfaces at larger contact angle hysteresis, or smaller contact angle at low surface sub-cooling degree. Experimenting with DWC heat transfer on a hybrid super-hydrophilic-hydrophobic network surface, Ji et al. [22] tested three kinds of super-hydrophilic-hydrophobic surfaces, with grid spacing at 1.5, 2.5 and 3.5 mm, and reporting that the hybrid super-hydrophilic-hydrophobic surface was capable of better controlling condensate droplet diameters, while the condensation heat transfer performance was superior to smooth hydrophobic and hydrophilic surfaces. In a similar experimental study, Oestreich et al. [23] considered the impact of hydrophilic constructal-like patterns on condensate mass flow rate production through a super-hydrophobic vertical test, including 5 designs, 3 of which had a branched topology with coated/uncoated area fractions around 30%, 50% and 70%, as well as fully-uncoated and fully-coated test areas. The results showed condensation rates to be achieved slightly higher for some experimental areas that with 70% coverage being super-hydrophobic. Moreover, Derby et al. [24] studied steam flow condensation in hybrid hydrophilic-hydrophobic micro-channels, and observed that steam condensation heat transfer coefficient for hydrophobic and hybrid patterned channels would be higher by a sizeable order of magnitude than hydrophilic surfaces. Also, Chatterjee et al. [25] showed condensation HTC of steam on a

surface with island patterns of hydrophilic and hydrophobic areas to be less than the hydrophobic surface, yet more than the hydrophilic surface at the same time. The impact of shape of pattern (island and tree patterns) and feature size on condensation HTC of steam underwent experimental measurement as well [26]. Davar et al. [27] experimentally investigated and measured the heat flux and heat transfer coefficient of condensation surfaces with hydrophobic and super-hydrophobic coatings, and reported that the Danphobix coating at 17 μm displayed the highest heat flux and heat transfer coefficient, and better performance than other coatings. Moreover, it was shown that a surface coated with Danphobix was a hybrid hydrophobic-hydrophilic surface, on which hydrophobic and hydrophilic areas were formed in a mixed manner and depending on the coating thickness. Davar et al. then proceeded to study the impacts of combining hydrophobic and hydrophilic copper and aluminium microparticles with Danphobix coating on parameters of heat flux and heat transfer coefficient [28]. The results attributed the best performance of condensation heat transfer to surfaces coated with Danphobix and mixed 3 weight percent of hydrophilic aluminium microparticles.

In this study, condensation on vertical hydrophobic-hydrophilic ptes was experimentally investigated. As coating methods of hybrid hydrophobic-hydrophilic surfaces have been addressed by previous researchers, the most important innovation of the present work would be producing a plate through a different method than those already introduced and experimented. Furthermore, promoting the condensation performance on the vertical plate generated by this hybrid hydrophobic-hydrophilic coating was also investigated.

2. Experimental setup

2.1 Experimental apparatus

The required experimental equipment comprised of steam generation system, cooling system, steam condensation system, and information control system in four modules, which were available at the Institute of Applied Hydrodynamics and Marine Technology of Iran University of Science and Technology (Hydrotech), as displayed in Fig. 1 [27].

The necessary experimental equipment to obtain the parameters as elaborated in the previous section comprised of systems for cooling, steam generation, steam condensation, and information control, depicted in the figure below.

For this purpose, distilled water was led via a diaphragm pump into a steam generator. Without a propeller, the pump was suitably resistant to cavitation, generated negligible vibrations and low-value stresses with the fluid, while the steam generator produced steam at 100℃. The steam was then guided through a super-heater for clarity and transparency, and the dry steam being led into a condensing chamber through a channel, where it condensed on a condensation test plate.

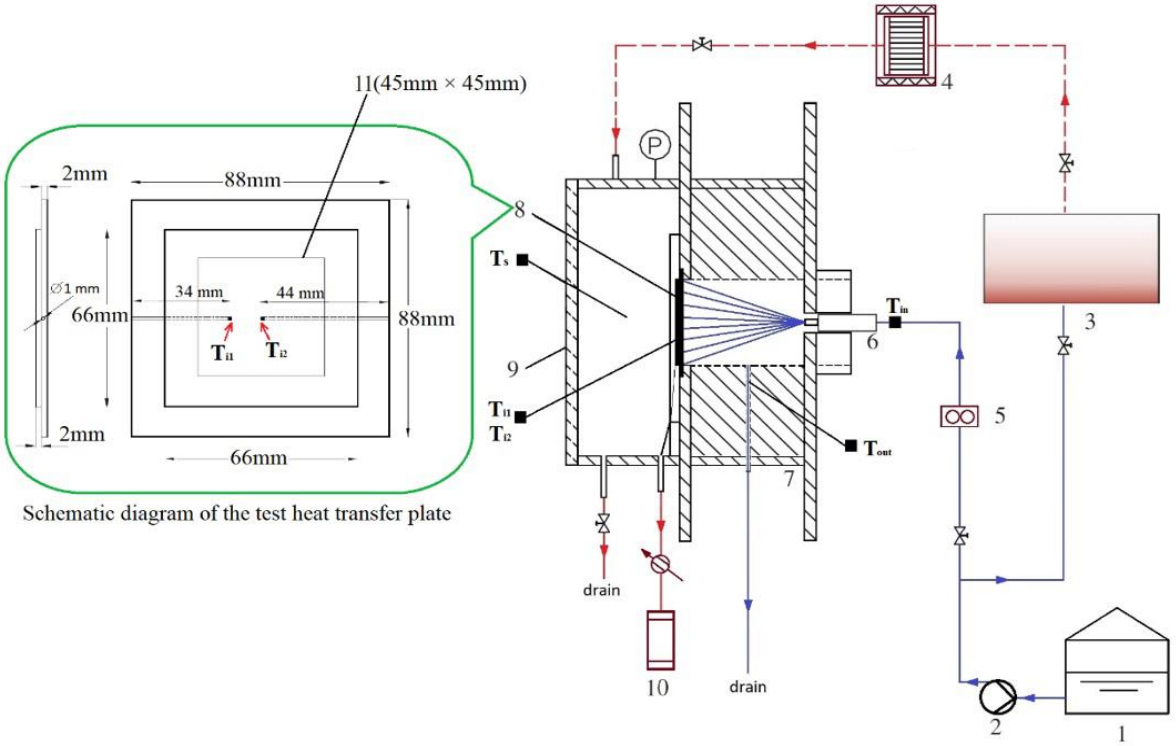

Figure 1. Schematic diagram of the experimental apparatus. 1-Deionized water tank; 2- Diaphragm pump; 3-Steam generator; 4-Superheater; 5- Rotameter; 6-Water spray nozzle; 7-Test section; 8- Heat transfer plate; 9- Glass window; 10- Measuring tube, 11- Area of plate in contact with steam. ■ Temperature measuring position; — Water line; - - - - - Steam line [27]

The velocity of the steam was calculated in the channel by division of volumetric flow rate into cross-section area of the channel. A platinum resistance thermometer (Pt 100), being an RTD type suitable for temperature range of -40+400°C, measured the steam temperature, with an error of ±0.1°C. The resistance in terms of temperature varied at 0.365 Ohm/°C. In order to measure the intake cooling water temperature, vapor entering the condensing chamber, and hot water from the plate cooling chamber, the RTD thermometers were all connected to the thermostats (SU_105PRR model of SAMWON ENG Company) with a PT100Ω sensor at temperature range of -200+400°C, and thermostat screens showing thermometers temperature at any given time. Two K-type thermocouples, on the other hand, were connected to the thermostats (SU-105KRR model of SAMWON ENG Company) with K(CA) sensor at the temperature range of -200+999°C, in order to measure the temperature inside the aluminium plate (T_{i1} & T_{i2}), while the thermostat screens showed instantaneous plate temperatures. A manometer with millibar precision monitored the steam pressure, being adjusted at atmospheric pressure using a valve at the end of the condensation chamber. During the warm-up period and before the test data was saved, the steam thus guided rapidly through the condensation chamber for a period of 60 minutes, so that the effect of non-condensing gas on the heat transfer would be eliminated. The plate was cooled with water from a cooling-water tank at constant temperature, by spraying the water passed through a flow-meter on the test plate backside using a pump and nozzle. The heat flux was supplied constantly and regularly for the heat transfer plate through pressure adjustment and the flux of cooling water. The present research revolved around on condensation in the absence of non-condensable gases, and the impact of non-condensable gases served among the critical parameters to affect condensation.

2.2 Heat transfer plate

A square aluminium plate was cut with the dimensions of 88×88 mm and thickness of 4 mm, and two holes (44 and 34 mm deep) were drilled into each side the plate, in order to install the thermocouples with the diameter of 1mm, measuring plate temperature. Furthermore, two thermocouples of Type K (NiCr-Ni) were placed in two holes at 2 mm from the condensing surface, in order to measure the temperature inside the aluminium plate. The thermocouple operated at a temperature range of -250+1000°C, and sensitivity at 46 μV/°C. The thermocouple of this type was selected for being relatively economical, humidity-resistant to a favourable degree, and suitable for low-temperature cases. Moreover, the temperature measuring error of the K-type thermocouple ranged at ±0.1°C. The front part of the aluminium plate was 66 × 66 mm2 and 2 mm thick, with an area of 45 × 45 mm designated for condensation, as exposed to the steam, bearing equal conditions for the uncoated and coated surfaces (Fig. 1).

2.3 Preparation of samples

Considering the high heat transfer of aluminium, favorable surface smoothness, popularity in industrial use, resistance to oxidation, high strength to weight ratio, and high surface energy, aluminium was selected as the base and principal material of the plates for dropwise condensation. First, a rolled coated aluminium plate was purchased at 3105 alloy and 2 mm thickness, and standard test samples of 66 × 66 mm2 were cut out of the plate. In order to minimize the adverse impacts of thermal tensions and the heat-affected zone (HAZ), the cutting process was conducted using the waterjet technology. As displayed in Fig. 2, aluminium plaques with standard dimensions were transformed through the following four-step process to the final plates for test in the condensation setup:

In the first step, the photolithography process was used to create a striped coating of positive photoresist (model S1813) on an area of 45 × 45 mm^2 on the sample surface. Consider the impacts of rectangular pattern dimensions, the optimal dimensions were extracted from previous studies and samples with different aspect ratios (length to width) were produced. Peng et al. [20] considered different widths of hydrophobic and hydrophilic areas in hybrid surfaces, and obtained the optimal widths, which were used for the purposes of the present study as well. Before the lithography process, the aluminium plate was washed with de-ionized water, acetone and propanol, and dried with clean dry air. Then, the positive photoresist (S1813) was spread over the aluminium surface through the spin coating method at 3,000 rpm for 30 seconds. The aluminium coated with the photoresist was pre-heated for 2 minutes at 95 ºC, then the mask of rectangular patterns prepared with a mask aligner was placed on the sample and UV radiated for 60 seconds at 1.4 mW/cm^2.

The photoresist was then washed in the developer solution, in order to wash off and remove the photoresist weakened by the UV radiation. Afterwards, a thin rectangular pattern of photoresist was re-cooked on the surface for final establishment for 1 minute at 95º C. As depicted in Fig. 2, the coated areas of the surface (with photoresist) would become resistant against HCl at the end of the first step, and would become resistant against acid corrosion in the second step, etching.

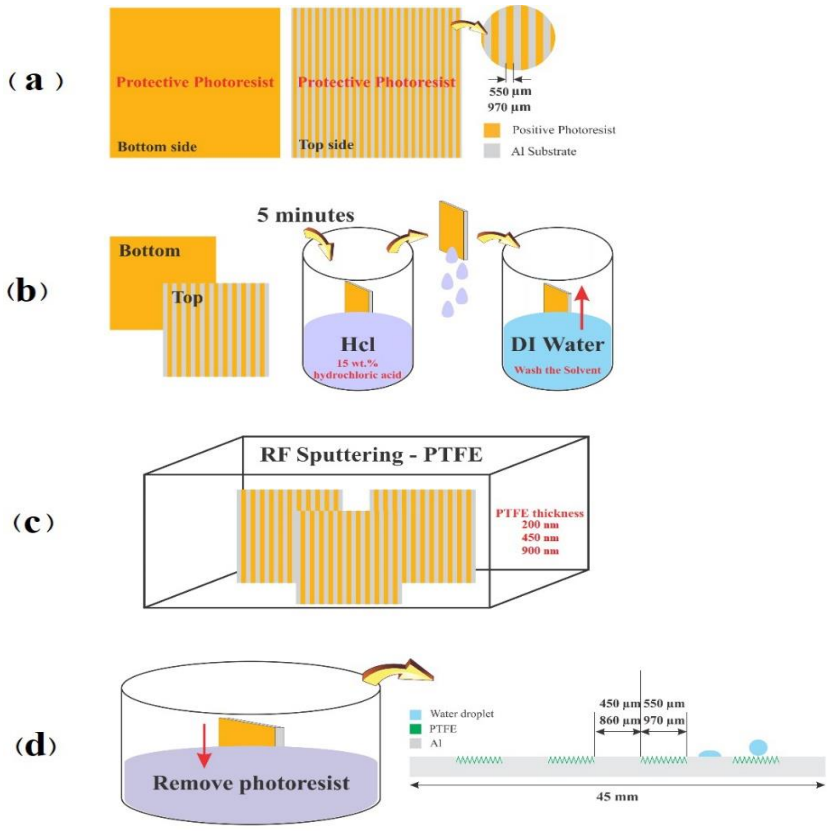

Figure 2. 4-step process of preparing dropwise condensation plate: A) placing a protective coating against the HCl acid on aluminium, using lithography; B) etching the samples in the HCl solution to create roughness on uncoated areas; C) PTFE sputtering on the entire surface; and D) removing the photoresist remaining on the surface

During the second step, the aluminium plate coated in HCl solution was etched, where the uncoated areas were corroded by the acid. The etching rate needed to be controlled to achieve the favorable surface roughness, and a separate experiment was thus conducted to measure the corrosion rate of aluminium in HCl solution. For that purpose, small plaques (1 cm2) of the aluminium plate were cut, washed with de-ionized water, acetone and propanol, and dried with clean dry air. A thin HCl solution at 15 % was prepared, and similar aluminium plaques were etched in it for 1-9 minutes. According to Fig. 3-a, the HCl solution left no tangible effect on the aluminium surface in Min. 1, yet traces of corrosion were observed along the rolling of the plate during Min. 2. From Min. 3 onward, almost the entire surface underwent corrosion, penetrating into the plaque.

Considering the need for low roughness and to prevent destruction of the photoresist layer on the aluminium, 110 seconds of etching in 15% HCl solution was experimentally identified as the optimal conditions for the etching process. After the etching, the samples were washed with de-ionized water and dried in a thermal furnace (for 2 hours at 70 ºC). As shown in Fig. 3-c, the third step included RF-sputtering of super-thin (below 1 µm) coatings of PTFE over the entire samples. For this purpose, the samples were placed inside the device and pre-vacuumed up to 1.9e-4 millibar, using a vacuum pump. The PTFE RF-sputtering was conducted in the presence of argon at 1.1e-2 millibar. Moreover, the process was fed by radio-frequency at 140 Watts. The produced layer depended on the time of sputtering.

The previous roughness of the surface before the PTFE sputtering, the adhesion of this polymer to the aluminium surface was guaranteed. Moreover, the precise thickness of this coating was also crucial to be considered. For that purpose, a control samples were also placed inside the device during the sputtering for the main plaques. After the sputtering, the PTFE thickness on the control samples was measured by a profile-meter. The PTFE layer thickness after one hour in the RF-sputtering was about 110 nm. Such small thickness would drastically reduce surface energy of aluminium and make it hydrophobic. Moreover, the surface beneath that coating was previously roughened, which facilitated adhesion to the surface and promoted its hydrophobicity.

In the last step, presented in Fig. 2-D, the lift-off process removed the entire photoresist remaining on the surface, leaving a surface with a striped microstructure with simultaneous hydrophilic and hydrophobic characteristics.

During the lift-off, the entire surface was first UV radiated, which destroyed the polymer structure of the photoresist on the surface.

The plaques were then washed in acetone to remove the remaining photoresist from the surface, except for the rough areas with PTFE coating.

The hydrophobic areas had controlled surface roughness and a super-thin coating of the PTFE polymer with low surface energy, while the hydrophilic ones were the original surface of the aluminium. The characteristics of the totally hydrophobic and hybrid hydrophobic-hydrophilic surfaces are presented in Table 1. Fig. 4 shows a sample hybrid hydrophobic-hydrophilic plate. In order to study the morphology of the final surfaces, SEM images of the condensation surfaces were produced. In accordance with Fig. 4c, the plate was comprised of parallel hydrophobic and hydrophilic areas. The hydrophobic areas included a PTFE coating with two advantages of porous morphology of the microstructure, and the low surface energy, both of which being effective in promoting hydrophobicity. The surface mapping analysis of the plates showed the entire surface to contain aluminium, while the PTFE-areas contained fluorine and carbon elements as well.

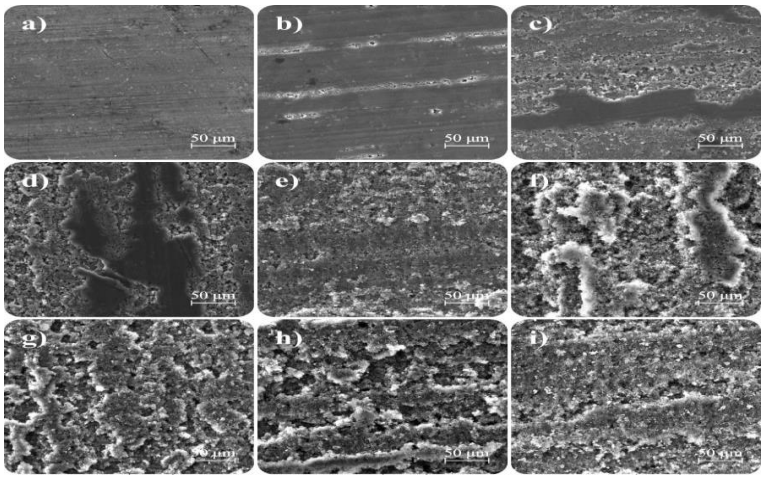

Figure 3. SEM images of etched aluminium plaques in 15% HCl solution, etched for 1 to 9 minutes in the acid (a to i)

Table 1. Plate Characteristics

No.	Surface Type	Width of Hydrophilic Area W_{dwc} (µm)	Width of Hydrophobic Area W_{fwc} (µm)	Thickness of Hydrophobic Coating (nm)
1	Totally Hydrophobic	0	45,000	200
2	Totally Hydrophobic	0	45,000	450
3	Totally Hydrophobic	0	45,000	900
4	Hybrid	450	550	200
5	Hybrid	450	550	450
6	Hybrid	450	550	900
7	Hybrid	860	970	200
8	Hybrid	860	970	450
9	Hybrid	860	970	900

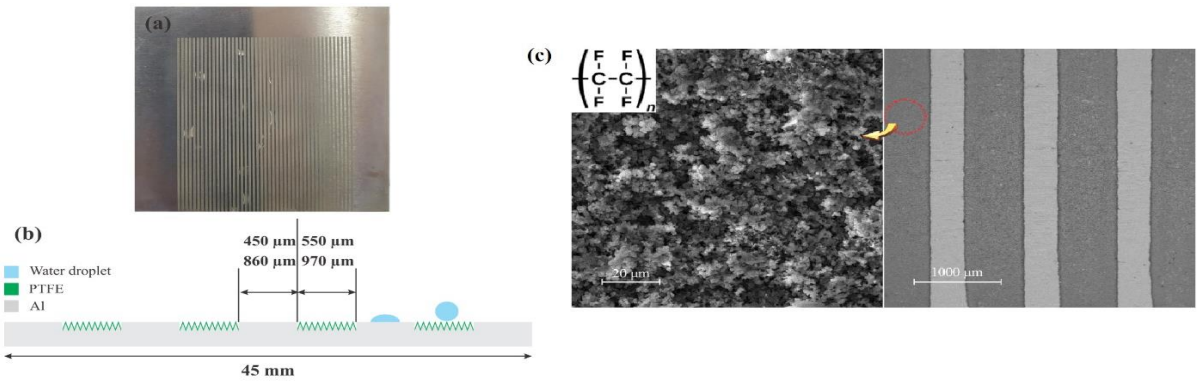

Figure 4. Dropwise Condensation Plate: a) Hybrid Hydrophilic-Hydrophobic Plate at 450 and 550 µm; b) Schematic Display of the Plate Cross-section and c) SEM Image of the Dropwise Condensation Surface: Right: Hydrophobic and Hydrophilic Areas; and Left: Porous Morphology of PTFE Polymer, Created by RF-sputtering of the PTFE Polymer Chain

2.4 Experimental data reduction

Calculations of this stage of the work included two main parameters, namely the heat flux q, and the temperature of condensing plate T_w. The heat from the condensing plate would be guided to the total cooling water behind the condensing plate, and the following relation would be used to calculate the condensation heat transfer rate [28]:

$$Q_1 = \frac{M.h_{fg}}{t} \quad (1)$$

here, M was condensate water mass on the test plate, and heat transfer rate was calculated by using the mass flow rate and temperature increase in the cooling water through the relation below [28]:

$$Q_2 = \dot{m}C_{p,l}(T_{out} - T_{in}) \quad (2)$$

here, $\dot{m}$ was the water mass flow rate inside the condenser, with the difference between Q_1 and Q_2 being below 6%. Imbalance between Q_1 and Q_2 called for taking an average into consideration for the upper and lower limits of the values.

The heat flux was therefore achieved through the following equation [28]:

$$q = \frac{Q_1 + Q_2}{2A} \quad (3)$$

The following equation provided averaged thermocouple position temperature ($T_{i\text{-}ave}$) [28]:

$$T_{i-ave} = \frac{T_{i1} + T_{i2}}{2} \quad (4)$$

T_{i1} and T_{i2} are thermocouple position temperatures as shown in Fig. 2.

The condensing surface temperature (T_w) was calculated through the relation below, which considered averaged thermocouple position temperature $T_{i\text{-}ave}$ and calculated heat flux q from the above relation [28]:

$$T_w = T_{i-ave} + q.\left(\frac{\Delta l_{Al}}{k_{Al}} + \frac{\Delta l_{Eq-coat}}{k_{coat}}\right) \quad (5)$$

Δl_{Al} represented the distance between measuring points of the thermocouples on the heat transfer plate and the aluminium surface. $\Delta l_{Eq\text{-}coat}$ was an equivalent thickness of the coating, in order to consider coating thermal resistance to calculate HTC using coating coverage. k_{Al} and k_{coat} stood for thermal conductivity of aluminium and coating, respectively, and HTC was obtained through the following equation [28]:

$$HTC = \frac{q}{\Delta T} = \frac{q}{T_s - T_w} \quad (6)$$

2.5 Uncertainty analysis

The general rules provided in ISO Guide to the Expression of Uncertainty in Measurement [29] were followed in order to resolve the experimental uncertainties in the experiment, and thus the combined uncertainty u_C was calculated for each variable, considering "Type A" and "Type B" components in accordance with Eq. (7) and Eq. (8).

$$u_C(y) = \sqrt{\sum_{i=1}^{n}\left(\frac{df}{dx_i}\right)^2 . u_{tot}^2(x_i)} \quad (7)$$

The global uncertainty for the measured data xi was assessed as:

$$u_{tot}^2(x_i) = u_A^2(x_i) + u_B^2(x_i) \quad (8)$$

The thermocouples position uncertainty was assumed at a negligible level, where $u_A(x_i)$ and $u_B(x_i)$ were Type A and Type B uncertainties, respectively, for the i-th variable x_i, while n being the total number of measured variables. Hence, Type A uncertainty was determined based on the probability distribution of values within the examined observations, and the most frequent and normal distribution was assumed, while Type B uncertainty related to the error propagation and instrumental properties. Type A uncertainty of the measured variables, including mass, water flow rate and temperatures, was calculated for this purpose according to Eq. (9) below:

$$u_A(x_i) = \frac{\sqrt{\frac{\sum_{j=1}^{m}\left(x_{i,j} - \frac{\sum_{j=1}^{m} x_{i,j}}{m}\right)^2}{m-1}}}{\sqrt{m}} \quad (9)$$

Here m stands for the number of data recorded by the relevant sensor, currently equal to 10.

Moreover, Instrument precision and related Type (B) uncertainty of the most measured variables are presented in Table 2. Finally, the expanded uncertainty $u_M(x_i)$ was obtained through multiplying $u_C(x_i)$ by a coverage factor k = 2.

The uncertainties of the thermodynamic variables in this analysis, being evaluated using NIST Refprop Version 9.1 were not considered [30], and the uncertainty propagation criterion dictated that the mean expanded uncertainties for temperature difference between steam and wall for all the data points, heat flux being removed in the measuring section and HTC were less than 3.7%, 4.7%, and 6.5% respectively, within the scope of the present experiment.

Table 2. Type B uncertainty of the measured parameters

Variable	Instrument Precision $E(y)$	Uncertainty $u_B(y) = E(y)/\sqrt{3}$
Temperature	±0.05 K	0.03%
Cooling water flow rate	±0.2 %	0.12%
Mass of condensate from the test plate (g)	±0.05 g	0.03%
Thickness and length of plate	±0.02 mm	0.01%
Time	±0.01 s	0.01%

2.6 Characterization

To measure static contact angle with water, a Plus 15 OCA Dataphysics was used at room temperature (25 ± 1 ºC), and some 5 µL pure de-ionized water was also used during the measurements. To obtain the contact angles, five measurements of five different points were conducted for each sample. For the dynamic contact angle measurements or the residual contact angle, the magnifying and minimizing method for the drop was employed, during which a drop of a certain size was placed on the sample. At a low speed, then, some fluid was injected into the drop and suctioned out, in order to calculate the advancing, receding and hysteresis angles. To measure the hysteresis contact angle, a JIKAN CAG-20 instrument designed by the science-based company Jikan Surface Nano-Engineering, from the University of Tehran.

The sample surfaces were analyzed by a Czech., Co Tescan, XMU II VEGA SEM microscope, before which a thin layer of silver was placed on the samples to promote the recording and imaging quality. The coating measurement was also conducted at the Micro-Electromechanical System laboratory of micro-technologies, Amirkabir University of Technology, using an Alpha-Step D-100 Stylus Profiler. The coating steps commenced with a mask aligner used in lithography process, and the RF-sputtering of the PTFE coating was also conducted at Mizan Microchip Techniques Company in Tehran. The measurements pertaining to condensation heat transfer coefficient and heat flux were conducted through a condensation parameter measurement instrument located at the Hydrotech Institute, Iran University of Science and Technology.

2.7 Validation

The laminar FWC on the vertical plate, and the assuptions pivoting on the Nusselt analysis helped the HTC to be expressed for the entire plate [31] in the Eq. 10. The HTC for the filmwise condensation on a vertical aluminium plate, on the other hand, was measured for the experimental setup designed, ensued by a comparison of the two modes (Fig. 5).

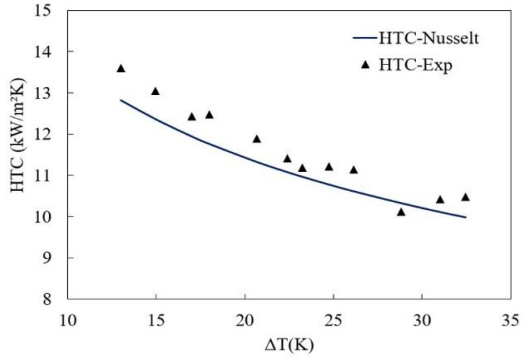

Figure 5. Comparison of HTC between Nusselt model and experimental values at various subcooling temperatures

The results showed that the HTC calculated from the experimental values provided for an acceptable error level at ±6%, which was relative to the Nusselt model. The solutions achieved by the experimental tests could therefore be considered as acceptably accurate.

$$HTC = 0.943\left[\frac{g\rho_l(\rho_l-\rho_v)k_l^3(h_{fg}+0.68C_{p,l}(T_{sat}-T_w))}{\mu_l(T_{sat}-T_w)L}\right]^{\frac{1}{4}} \quad (10)$$

3. Results

3.1 Contact Angles

The maximum radius of droplets during a complete DWC process, and the DWC heat transfer in turn, are directly affected by the wettability properties of solid surfaces, including contact angle and contact angle hysteresis. On a surface, contact angle hysteresis (Δθ) can be defined as the difference between the advancing (θ_a) and receding (θ_r) contact angles, or $\Delta\theta = \theta_a - \theta_r$. On the hydrophobic region, the static contact angle of water is measured around 154°C ± 5°C, and around 50°C ± 5°C on the hydrophilic region, while the contact angle hysteresis (advancing contact angle minus receding contact angle) may reach to around 41°C. The measurements of different coating thicknesses depicted no significant differences in contact angles. On the other hand, the values showed that under increased coating thickness, the contact angle and contact angle hysteresis increased and decreased with negligible differences, respectively.

3.2 Roughness

Fig. 6 portrays the roughness topography of plaques with a hydrophobic region of 860 µm wide and different thicknesses, a completely hydrophobic plaque, and one with a hydrophobic region of 450 µm wide and uniform thickness of 400 nm.

The average roughness of plaques with a hydrophobic region of 860 µm wide and coating thicknesses of 200, 450 and 900 µm was 7.3, 5.2 and 7.1 µm, respectively. For the plaque with a hydrophobic region of 450 µm wide and uniform thickness of 400 nm, the average roughness was 6.1 and 5.4 µm, respectively, and it appeared that the average roughness of all surfaces was approximately similar. According to the results, the lowest average roughness value belonged to the plaque with a hydrophobic region of 450 µm wide and thickness of 400 nm. The negligible difference in roughness average of the plaques could partly be attributed to the fact that all plaques were made of identical coating materials.

3.3 DWC Parameters

At this stage of the work, all the surfaces were placed in the condensation chamber, and were subject to condensation in accordance with their different characteristics.

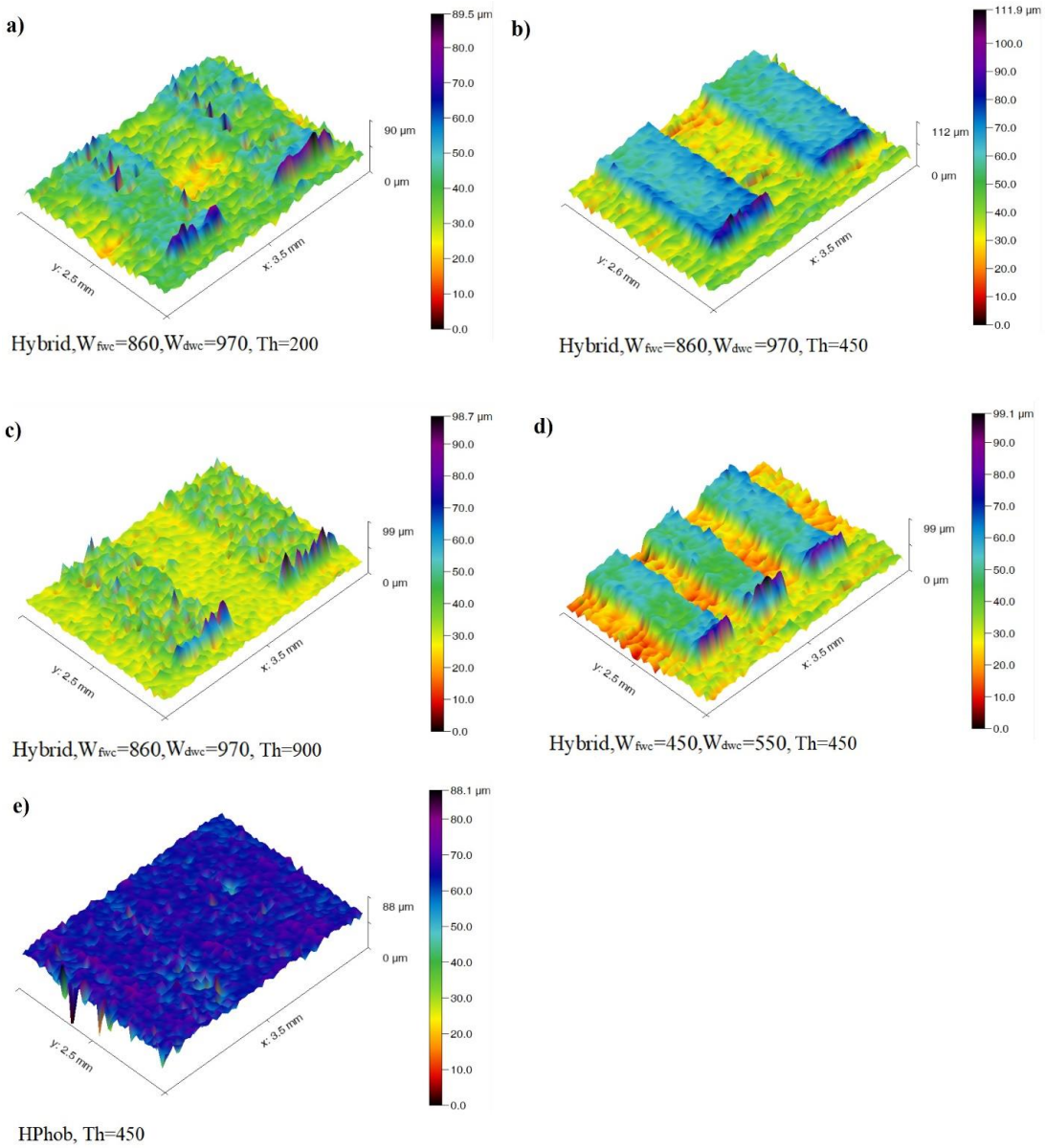

Figure 6. surface roughness profiles for a=Hybrid- W_{fwc}=860 µm- W_{dwc}=970 µm- Th=200 µm, b= Hybrid- W_{fwc} =860 µm- W_{dwc} =970 µm- Th=450 µm, c= Hybrid- W_{fwc} =860 µm- W_{dwc} =970 µm- Th=900 µm, d= Hybrid- W_{fwc} =450 µm- W_{dwc} =550 µm- Th=450 µm, e=HPhob, Th=450 µm.

The relevant information, such as the thermocouple temperatures, flow rate of the cooling water and condensed water for each test was gathered, and the tests were performed for 10 times to ensure reliability of the results and prevent errors, the average of which were presented as the test results.

Using the mentioned information, the heat transfer coefficient and heat flux for each surface were obtained, in order to determine the optimum conditions. As elaborated in Table 1, three types of surfaces were tested with different roughness and hydrophobicity, under the coatings of 200, 450 and 900 nm.

The first type was a totally hydrophobic surface, the second a hybrid hydrophobic-hydrophilic surface (width of 450 µm for hydrophilic area and 550 µm for the hydrophobic), and the third a hybrid hydrophobic-hydrophilic surface (width of 860 µm for hydrophilic area and 970 µm for the hydrophobic), which were placed under equal conditions at the condensation chamber. The second surface type included 45% hydrophilic and 55% hydrophobic areas, while third type was composed of 47% and 53% hydrophilic and hydrophobic areas, respectively.

Fig. 7 depicts the formation condensed drops on each surface, where it could be observed that surface hydrophobicity grows with increased coating thickness.

At the same time, the diameter of drops decreases at the falling threshold, which in turn results in reduced heat resistance along the heat transfer between the cooled area behind the plate and the area exposed to the steam, and thus improved heat transfer.

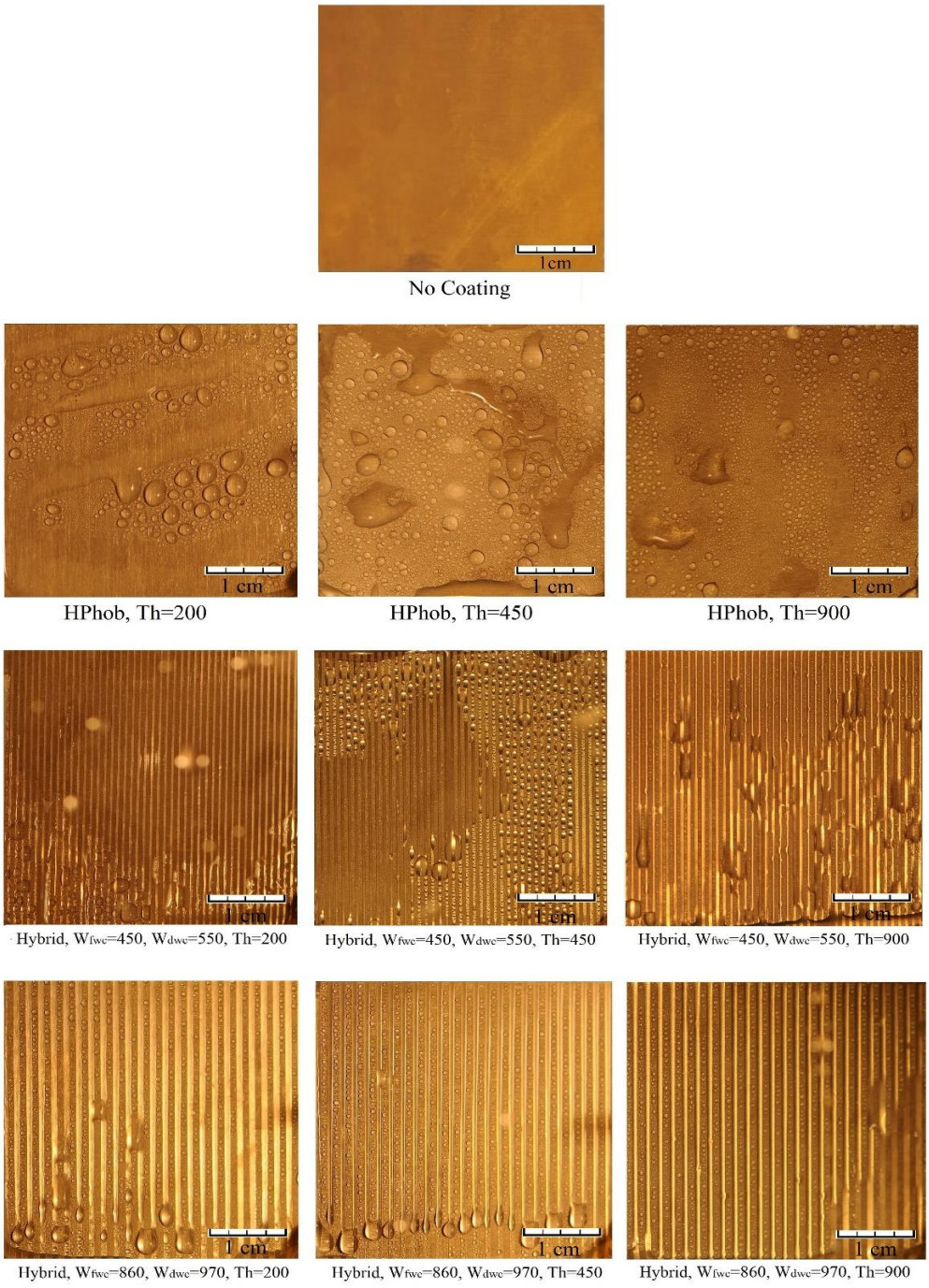

Figure 7. Condensation formation on hydrophobic, hybrid (hydrophilic-hydrophobic) and uncoated surfaces

On the other hand, the reduced diameters emanate from the increased coating thickness, which further results in heat resistance along the heat transfer path. Moreover, besides the above positive and negative points along the condensation heat transfer, the roughness geometry and surface hydrophobicity could also be crucial in determining the principal parameters of condensation heat transfer, such as the heat flux and heat transfer coefficient.

The graphs for condensation heat transfer coefficient and heat flux at different cooling temperatures of the surface are presented in Fig. 8 and 9, respectively. The maximum error of all the data was taken into consideration (max. 7%), yet the error percentage of the heat flux and HTC values could not be displayed in the figure due to the detection of points. The values of condensation heat transfer coefficient and heat flux for the three surface types can be seen to be higher for the coating at 450 nm, than the other two thickness values. The results show that by increasing coating thickness from 200 to 450 nm, the positive impact of smaller drops forming due to increased coating thickness outweighed the negative impact exerted by the increased heat resistance along the condensation heat transfer path, and resulted in higher condensation heat transfer coefficient and heat flux.

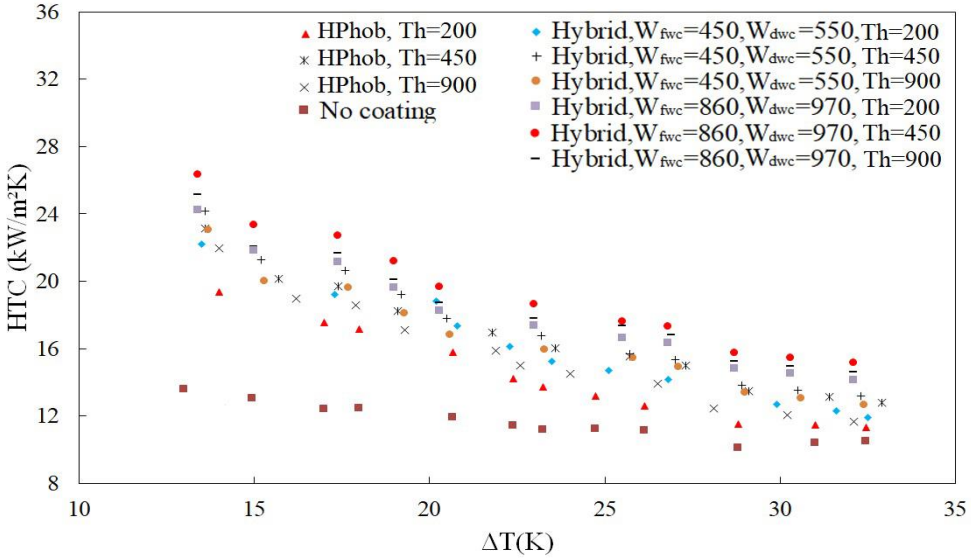

Figure 8. HTC versus various subcooling temperatures

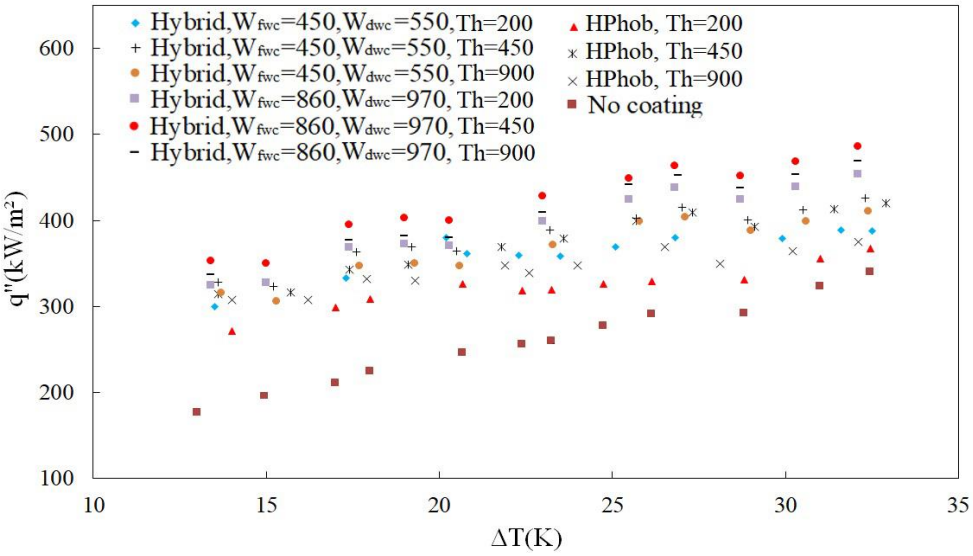

Figure 9. Heat flux versus various subcooling temperatures

When the coating thickness was increased from 450 to 900 nm, on the other hand, the positive impact of smaller drops forming due to increased coating thickness was inferior to the negative impact exerted by the increased heat resistance along the condensation heat transfer path, which resulted in lower condensation heat transfer coefficient and heat flux. The values of condensation heat transfer coefficient and heat flux on the hybrid hydrophobic-hydrophilic surface of the third type (width of 860 µm for hydrophilic area and 970 µm for the hydrophobic, and thickness of 450 nm) increased by 1.44-2.01 and 1.43-1.81 times, respectively, compared to the uncoated surface. Compared to the uncoated surface, moreover, the two parameters increased by 1.25-1.68 and 1.26-1.85 times, respectively, for the hybrid hydrophobic-hydrophilic surface of the second type (width of 450 µm for hydrophilic area and 550 µm for the hydrophobic, and thickness of 450 nm), and 1.11-1.68 and 1.10-1.61 times, respectively, for the totally hydrophobic surface.

The obtained results showed that despite having the smaller hydrophobic area, the hybrid hydrophobic-hydrophilic surface of the third type (width of 860 µm for hydrophilic area and 970 µm for the hydrophobic, and thickness of 450 nm) displayed the highest values of condensation heat transfer coefficient and heat flux, than the other two surfaces, namely the hybrid hydrophobic-hydrophilic surface of the second type (width of 450 µm for hydrophilic area and 550 µm for the hydrophobic, and thickness of 450 nm), and the totally hydrophobic surface. In fact, the width of 860 µm for hydrophilic area provided for better removal of condensed drops from the surface.

On the other hand, increasing the plate contact angle in such surfaces, similar to the totally hydrophobic

surface, increased the values of condensation heat transfer coefficient and heat flux until the optimum coating thickness of 450 nm, yet the mentioned value fell when the thickness further increased to 900 nm.

During the condensation test experiment (180 hours), the coating practically maintained its durability, meaning that after 50 condensation tests in a course of 6 months, the values of parameters q and HTC only fell by 6%, and the durability of the coating was therefore considered as constant.

Conclusions

- In the present study, three surface types were produced, including a totally hydrophobic surface, a hybrid hydrophobic-hydrophilic surface with the width of 550 μm for the hydrophobic area, and a hybrid hydrophobic-hydrophilic surface with the width of 970 μm for the hydrophobic area. The second surface type included 45% hydrophilic and 55% hydrophobic areas, while third type was composed of 47% and 53% hydrophilic and hydrophobic areas, respectively.

  The three surface types were produced at three coating thicknesses of 200, 450 and 900 nm.
- Using the 4-step process below, the aluminum plaques at standard dimensions were transformed for the test in the condensation setup into to the final plates (Fig. 3): applying a protective coating on aluminum against the HCl acid (lithography); creating roughness on the uncoated areas by etching the samples in the HCl solution; sputtering the entire surface with PTFE; and cleaning the surface of the photoresist remaining.
- Increasing the coating thickness leads to higher surface hydrophobicity, and reduced diameter of drops at the falling threshold, which in turn results in reduced heat resistance along the heat transfer path, and thus improved heat transfer. On the other hand, the increased coating thickness further generates heat resistance along the heat transfer path.
- The results showed that the highest values of condensation heat transfer coefficient and heat flux were observed at the coating thickness of 450 nm. By increasing coating thickness from 200 to 450 nm, the positive impact of smaller drops forming due to increased coating thickness outweighed the negative impact exerted by the increased heat resistance along the condensation heat transfer path, and resulted in higher condensation heat transfer coefficient and heat flux.
- When the coating thickness was increased from 450 to 900 nm, on the other hand, the positive impact of smaller drops forming due to increased coating thickness was inferior to the negative impact exerted by the increased heat resistance along the condensation heat transfer path, which resulted in lower condensation heat transfer coefficient and heat flux.
- The highest values of condensation heat transfer coefficient and heat flux were observed on the hybrid hydrophobic-hydrophilic surface (width of 860 μm for hydrophilic area and 970 μm for the hydrophobic, and thickness of 450 nm), which increased by 1.44-2.01 and 1.43-1.81 times, respectively, compared to the uncoated surface.

Nomenclature

A	condensing surface area, m^2
$C_{p,l}$	specific heat of water, J/ (kg °C)
DWC	dropwise condensation
FWC	filmwise condensation
HTC	heat transfer coefficient, $W/(m^2\ °C)$
h_{fg}	latent heat of vaporization, J/kg
Δl	distance, m
M	mass of condensate from the test plate, kg
$\dot{m}$	mass flow rate of water in condenser, kg/s
Q	heat transfer rate, W
q	heat flux, W/m^2
t	experimental time, s
T_i	thermocouple position temperature, °C
T_{in}	inlet water temperature, °C
T_{out}	outlet water temperature, °C
T_s	steam temperature, °C
T_w	surface temperature, °C
Th	thickness, m
u_A	type-A uncertainty, %
u_B	type-B uncertainty, %
u_C	combined uncertainty, %
u_M	expanded uncertainty, %
W_{FWC}	filmwise region width, m
W_{DWC}	dropwise region width, m

Acknowledgements

The authors would like to thank the members of the Institute of Applied Hydrodynamics and Marine Technology of Iran University of Science and Technology (Hydrotech), for their cooperation in conducting the tests for the present research.

References

[1] Ferreira, J.C.A. and Barbosa, J.R., 2020. Quantifying interfacial parameters of upward and downward annular flow condensation from high-speed visualization, J Braz. Soc. Mech. Sci. Eng., 42(158).

[2] Li, B., Feng, L., Wang, L. and Dai, Y., 2021. Experimental investigation of condensation heat transfer and pressure drop of R152a/R1234ze(E)

in a smooth horizontal tube, Heat Transfer Research, 52 (7), pp.35-54.

[3] Ko, J.W., Jeon, D.S. and Kim, Y.L., 2018. Experimental study on film condensation heat transfer characteristics of R1234ze(E) and R1233zd(E) over horizontal plain tubes, J Mech Sci Technol., 32, pp.527–534.

[4] Rao, Y., Li, H., Shen, S., Yang, Q., Zhang, G., Zhang, X., Li, M. and Duan, S., 2017. Water vapor condensation on the inner surface of an N95 filtering facepiece respirator, Heat Transfer Research, 50(3), pp.217-231.

[5] Farahani, S.D. and Karami, M., 2019. Experimental estimation of local heat flux on boiling surface in a mini-channel, Int. J. Communications in Heat and Mass Transfer. 108, 104271.

[6] Farahani, S.D. and Kowsary, F., 2012. Estimation local convective boiling heat transfer coefficient in mini channel, Int. J. Communications in Heat and Mass Transfer, 39(2), pp.304-310.

[7] Karami, M., Davoodabadi Farahani, S., Kowsary, F. and Mosavi, A. 2020. Experimental estimation of temporal and spatial resolution of coefficient of heat transfer in a channel using inverse heat transfer method, Engineering Applications of Computational Fluid Mechanics, 14(1), pp.271-283.

[8] Davar, H., Nouri, N.M. and Navidbakhsh, M., 2021. Enhancement of condensation heat transfer at aluminum surfaces via laser-induced surface roughening, J Braz. Soc. Mech. Sci. Eng., 43(346).

[9] Schmidt, E., Schurig, W. and Sellschopp, W., 1930. Condensation of water vapour in film-and drop form, Zeitschrift Des Vereines Deutscher Ingenieure, 74, pp.544-544.

[10] Citakoglu, E., and Rose, J.W., 1968. Dropwise condensation-some factors influencing the validity of heat-transfer measurements, Int. J. Heat Mass Transf., 11(3), pp.523-537.

[11] Izumi, M., Kumagai, S., Shimada, R., and Yamakawa, N., 2004. Heat transfer enhancement of dropwise condensation on a vertical surface with round shaped grooves, Exp. Therm. Fluid Sci., 49(2), pp.243-248.

[12] Koch, G., Zhang, D.C., and Leipertz, A., 1997. Condensation of steam on the surface of hard coated copper discs, Heat and Mass Transfer., 32(22), pp.149-156.

[13] Majumdar, A., and Mezic, I., 1999. Instability of ultra-thin water films and the mechanism of droplet formation on hydrophilic surfaces," J. Heat Mass Transf., 121(4), pp.964-971.

[14] Vemuri, S., and Kim, K.J., 2006. An experimental and theoretical study on the concept of dropwise condensation, Int. J. Heat Mass Transf., 49(3), pp.649-657.

[15] Tianqing, L., Chunfeng, M. Xiangyu, S. and Songbai, X., 2007. Mechanism study on formation of initial condensate droplets, The American Institute of Chemical Engineers Journal, 53(4), pp.1050–1055.

[16] Ma, X.-H., Zhou, X.-D., Lan, Z., Yi-Ming, L.I., and Zhang, Y., 2008. Condensation heat transfer enhancement in the presence of non-condensable gas using the interfacial effect of dropwise condensation, Int. J. Heat Mass Transf., 51(7), pp.1728-1737.

[17] Boreyko, J.B., and Chen, C.-H., 2009. Self-propelled dropwise condensate on superhydrophobic surfaces, Phys. Rev. Lett., 103(18), 184501.

[18] Talesh Bahrami, H.R., Azizi, A. and Saffari, H., 2020. An Empirical Study on Dropwise Condensation Occurred on Surfaces Hydrophobized Using a Single-Step Electrodeposition, Amirkabir Journal of Mechanical Engineering, 52(6), pp.1397-1412.

[19] Ghosh, A., Beaini, S., Zhang, B.J., Ganguly, R., and Megaridis, C.M., 2014. Enhancing Dropwise Condensation through Bioinspired Wettability Patterning, Langmuir, 30, pp.13103-13115.

[20] Peng, B., Ma, X., Lan, Z., Xu, W., and Wen, R., 2015. Experimental investigation on steam condensation heat transfer enhancement with vertically patterned hydrophobic–hydrophilic hybrid surfaces, Int. J. Heat Mass Tran., 83(4), pp.27-38.

[21] Peng, B., Ma, X., Lan, Z., Xu, W., and Wen, R., 2014. Analysis of condensation heat transfer enhancement with dropwise-filmwise hybrid surface: Droplet sizes effect, Int. J. Heat Mass Trans., 77, pp.785–794.

[22] Ji, X., Zhou, D., Dai, C., and Xu, J., 2019. Dropwise condensation heat transfer on superhydrophilic-hydrophobic network hybrid surface, Int. J. Heat Mass Trans., 132, pp.52-67.

[23] Oestreich, J.L., van der Geld, C.W.M., Oliveira, J.L.G. and da Silva, A.K., 2019. Experimental condensation study of vertical superhydrophobic surfaces assisted by hydrophilic constructal-like patterns, International Journal of Thermal Sciences, 135, pp.319–330.

[24] Derby, M.M. Chatterjee, A., Peles, Y. and Jensen, M.K., 2014. Flow condensation heat transfer enhancement in a mini-channel with hydrophobic and hydrophilic patterns, Int. J. Heat Mass Trans., 68, pp.151–160.

[25] Chatterjee, A., Derby, M.M. Peles, Y. and Jensen, M.K., 2013. Condensation heat transfer on patterned surfaces, Int. J. Heat Mass Trans., 66, pp.889–897.

[26] Chatterjee, A., Derby, M.M., Peles, Y., and Jensen, M.K., 2014. Enhancement of condensation heat transfer with patterned surfaces, Int. J. Heat Mass Trans., 71, pp.675– 681.

[27] Davar, H., Nouri, N.M. and Navidbakhsh, M., 2021. Effects of Superhydrophobic, Hydrophobic and Hybrid Surfaces in Condensation Heat Transfer, Journal of Applied Fluid Mechanics, 14(4), pp.1077-1090.

[28] Davar, H., Nouri, N.M., Navidbakhsh, M., Sekhavat, S. and Ansari, A., 2021. Enhancement of dropwise condensation heat transfer on hydrophilic-hydrophobic hybrid surface using microparticles, Experimental Heat Transfer, 35(4), pp.535-552.

[29] ISO Guide to the Expression of Uncertainty in Measurement, 1995.

[30] Lemmon, E.W., Huber, M.L., and McLinden, M.O., 2013. NIST Standard Reference Database 23: Reference Fluid Thermodynamic and Transport Properties-REFPROP, Version 9.1.

[31] Bergman, T.L., Lavine, A.S., Incropera, F.P. and Dewitt, D.P., 2011. Fundamentals of Heat and Mass Transfer.